



# Role of OH variability in the stalling of the global atmospheric CH<sub>4</sub> growth rate from 1999 to 2006

Joe McNorton<sup>1,2</sup>, Martyn P. Chipperfield<sup>1,2</sup>, Manuel Gloor<sup>3</sup>, Chris Wilson<sup>1,2</sup>, Wuhu Feng<sup>1,4</sup>, Garry D. Hayman<sup>5</sup>, Matt Rigby<sup>6</sup>, Paul B. Krummel<sup>7</sup>, Simon O'Doherty<sup>6</sup>, Ronald G. Prinn<sup>8</sup>, Ray F. Weiss<sup>9</sup>, Dickon Young<sup>6</sup>, Ed Dlugokencky<sup>10</sup>, and Steve A. Montzka<sup>10</sup>

<sup>1</sup>School of Earth and Environment, University of Leeds, Leeds, LS2 9JT, UK

<sup>2</sup>National Centre for Earth Observation, University of Leeds, Leeds, LS2 9JT, UK

<sup>3</sup>School of Geography, University of Leeds, Leeds, LS2 9JT, UK

<sup>4</sup>National Centre for Atmospheric Science, University of Leeds, Leeds, LS2 9JT, UK

<sup>5</sup>Centre for Ecology and Hydrology, Wallingford, UK

<sup>6</sup>School of Chemistry, University of Bristol, Bristol, BS8 1TS, UK

<sup>7</sup>CSIRO Oceans and Atmosphere Flagship, Aspendale, Victoria, Australia

<sup>8</sup>Center for Global Change Science, Massachusetts Institute of Technology, Cambridge, MA 02139, USA

<sup>9</sup>Scripps Institution of Oceanography, University of California, San Diego, CA 92093, USA

<sup>10</sup>National Oceanic and Atmospheric Administration, Boulder, CO, USA

Correspondence to: Joe McNorton (eejrm@leeds.ac.uk)

Received: 17 December 2015 – Published in Atmos. Chem. Phys. Discuss.: 18 January 2016

Revised: 9 June 2016 – Accepted: 10 June 2016 – Published: 30 June 2016

**Abstract.** The growth in atmospheric methane (CH<sub>4</sub>) concentrations over the past 2 decades has shown large variability on a timescale of several years. Prior to 1999 the globally averaged CH<sub>4</sub> concentration was increasing at a rate of 6.0 ppb yr<sup>-1</sup>, but during a stagnation period from 1999 to 2006 this growth rate slowed to 0.6 ppb yr<sup>-1</sup>. From 2007 to 2009 the growth rate again increased to 4.9 ppb yr<sup>-1</sup>. These changes in growth rate are usually ascribed to variations in CH<sub>4</sub> emissions. We have used a 3-D global chemical transport model, driven by meteorological reanalyses and variations in global mean hydroxyl (OH) concentrations derived from CH<sub>3</sub>CCl<sub>3</sub> observations from two independent networks, to investigate these CH<sub>4</sub> growth variations. The model shows that between 1999 and 2006 changes in the CH<sub>4</sub> atmospheric loss contributed significantly to the suppression in global CH<sub>4</sub> concentrations relative to the pre-1999 trend. The largest factor in this is relatively small variations in global mean OH on a timescale of a few years, with minor contributions of atmospheric transport of CH<sub>4</sub> to its sink region and of atmospheric temperature. Although changes in emissions may be important during the stagnation period, these results imply a smaller variation is required to explain the

observed CH<sub>4</sub> trends. The contribution of OH variations to the renewed CH<sub>4</sub> growth after 2007 cannot be determined with data currently available.

## 1 Introduction

The global mean atmospheric methane (CH<sub>4</sub>) concentration has increased by a factor of 2.5 since the pre-industrial era, from approximately 722 ppb in 1750 to 1803.2 ± 0.7 ppb in 2011 (Etheridge et al., 1998; Dlugokencky et al., 2005). Over this time period methane has accounted for approximately 20 % of the total direct anthropogenic perturbation of radiative forcing by long-lived greenhouse gases (0.48 ± 0.05 W m<sup>-2</sup>), the second-largest contribution after CO<sub>2</sub> (Cicerone and Oremland, 1988; Myhre et al., 2013). This long-term methane increase has been attributed to a rise in anthropogenic emissions from fossil fuel exploitation, agriculture, waste management, and biomass burning (Dlugokencky et al., 2011). Predictions of future CH<sub>4</sub> levels require a complete understanding of processes governing emissions and atmospheric removal.

Since the mid-1980s measurements of CH<sub>4</sub> in discrete atmospheric air samples collected at surface sites have been used to observe changes in the interannual growth rate of CH<sub>4</sub> (Rigby et al., 2008; Dlugokencky et al., 2011; Kirschke et al., 2013). Nisbet et al. (2014) showed that between 1984 and 1992 atmospheric CH<sub>4</sub> increased at  $\sim 12$  ppb yr<sup>-1</sup>, after which the growth rate slowed to  $\sim 3$  ppb yr<sup>-1</sup>. In 1999 a period of near-zero growth began which continued until 2007. In 2007 this stagnation period ended, and up until 2009 average growth increased again to  $\sim 4.9$  ppb yr<sup>-1</sup> (Rigby et al., 2008; Dlugokencky et al., 2011).

The reasons for the pause in CH<sub>4</sub> growth are not well understood. Bousquet et al. (2006) performed an atmospheric transport inversion study to infer an increase in anthropogenic emissions since 1999. Similarly, the Emissions Database for Global Atmospheric Research (EDGAR) v3.2 bottom-up anthropogenic emission inventory, an updated inventory to that used as an *a priori* by Bousquet et al. (2006), shows a year-on-year increase in anthropogenic CH<sub>4</sub> emissions between 1999 and 2006 (Olivier et al., 2005). This would suggest that a decrease in anthropogenic emissions is not the likely cause of the pause in growth during this period. A second potential explanation is a reduction in wetland emissions between 1999 and 2006, which is in part compensated by an increase in anthropogenic emissions (Bousquet et al., 2006). However, more recently, Pison et al. (2013) used two atmospheric inversions alongside a process-based model and found much more uncertainty in the role wetlands played in the pause in growth over this period. Their study found a negative trend in Amazon Basin emissions between 2000 and 2006 from the process-based model and a positive trend from the inversion estimates.

Dlugokencky et al. (2003) argued that the behaviour of global mean CH<sub>4</sub> up to around 2002 was characteristic of the system approaching steady state, accelerated by decreasing emissions at high northern latitudes in the early 1990s and fairly constant emissions elsewhere. However, since then there have been notable perturbations to the balance of sources and sinks (Rigby et al., 2008). The observed growth since 2007 has been, at least partly, attributed to increases in wetland (Bousquet et al., 2011) and anthropogenic emissions (Bousquet et al., 2011). Recent changes in emissions are not well constrained, and the reasons for the renewed growth are also not fully understood (Nisbet et al., 2014).

Atmospheric chemistry has also been hypothesised to play a role in past variations in CH<sub>4</sub> growth rates. The major (90 %) sink of atmospheric CH<sub>4</sub> is via reaction with the hydroxyl radical, OH. Variations in the global mean concentration of OH ([OH]), or changes to the reaction rate through changes in temperature, therefore have the potential to affect CH<sub>4</sub> growth. Previous studies have suggested that an increase in atmospheric OH concentration may have been at least partly responsible for a decrease in the CH<sub>4</sub> growth rate (Karlsdottir and Isaksen, 2000; Lelieveld et al., 2004; Wang et al., 2004; Fiore et al., 2006). This rise in OH has been at-

tributed to an increase in lightning NO<sub>x</sub> (Fiore et al., 2006), a decrease in column O<sub>3</sub> (Wang et al., 2004), and changes in atmospheric pollutants (Karlsdottir and Isaksen, 2000). The abundance of other species such as H<sub>2</sub>O and CH<sub>4</sub> also determines the concentration of OH (Lelieveld et al., 2004). Prinn et al. (2005) and Voulgarakis et al. (2015) suggested that major global wildfires and El Niño–Southern Oscillation (ENSO) events could influence [OH] variability.

Warwick et al. (2002) investigated the impact of meteorology on atmospheric CH<sub>4</sub> growth rates from 1980 to 1998, i.e. well before the observed recent pause. They concluded that atmospheric conditions could be an important driver in the interannual variability (IAV) of atmospheric CH<sub>4</sub>. In similar studies a combination of atmospheric dynamics and changes in emissions were shown to explain some of the earlier past trends in atmospheric CH<sub>4</sub> (Fiore et al., 2006; Patra et al., 2009). This paper builds on these studies to investigate the chemical and non-chemical atmospheric contribution to the recent variations in CH<sub>4</sub> growth. By “non-chemical” we mean transport-related influences, although the loss of CH<sub>4</sub> is ultimately due to chemistry as well. We use a 3-D global chemical transport model (CTM) to simulate the period from 1993 to 2011 and to quantify the impact of variations in [OH] and meteorology on atmospheric CH<sub>4</sub> growth.

## 2 Data and models

### 2.1 NOAA and AGAGE CH<sub>4</sub> data and derived OH

We have used surface CH<sub>4</sub> observations from 19 National Oceanographic and Atmospheric Administration/Earth System Research Laboratory (NOAA/ESRL) cooperative global air sampling sites (Dlugokencky et al., 2014) over 1993–2009 (see Table 1). To calculate the global average concentration, measurements were interpolated across 180 latitude bins, which were then weighted by surface area. We have also used the same method to derive global mean CH<sub>4</sub> based on five sites from the Advanced Global Atmospheric Gases Experiment (AGAGE) network (Prinn et al., 2000, 2015; Cunnold et al., 2002).

Montzka et al. (2011) used measurements of methyl chloroform (CH<sub>3</sub>CCl<sub>3</sub>) from an independent set of flasks sampled approximately weekly at a subset of NOAA air sampling sites to derive global [OH] anomalies from 1997 to 2007 and found only a small interannual variability ( $2.3 \pm 1.5$  %). They argued that uncertainties in emissions are likely to limit the accuracy of the inferred interannual variability in global [OH], particularly before 1997. At that time the emissions were large but decreasing rapidly due to the phaseout of CH<sub>3</sub>CCl<sub>3</sub> production and consumption, and the large atmospheric gradients were also more difficult to capture accurately with only few measurement sites. Instrument issues caused an interruption to their CH<sub>3</sub>CCl<sub>3</sub> time series in 2008–2009. We have averaged these (based on the red curve in

**Table 1.** List of NOAA and AGAGE stations which provided CH<sub>4</sub> and CH<sub>3</sub>CCl<sub>3</sub> observations.

Site code	Site name	Lat. (° N)	Lon. (° N)	Altitude (km)	CH <sub>4</sub>	CH <sub>3</sub> CCl <sub>3</sub>	Start date <sup>a</sup>	End date
ABP	Arembepe, Brazil	−12.77	−38.17	0	NOAA		27 Oct 2006	12 Jan 2010
ALT	Alert, Canada	82.45	−62.51	0.2	NOAA	NOAA	10 Jun 1985	Ongoing
ASC	Ascension Island, UK	7.97	−14.4	0.09	NOAA		11 May 1983	Ongoing
BRW	Barrow, USA	71.32	−156.61	0.01	NOAA	NOAA	6 Apr 1983	Ongoing
CGO	Cape Grim, Australia	−40.68	144.69	0.09	NOAA/AGAGE	NOAA/AGAGE	19 Apr 1984	Ongoing
HBA	Halley Station, UK	−75.61	−26.21	0.03	NOAA		17 Jan 1983	Ongoing
ICE	Storhofdi, Iceland	63.4	−20.29	0.12	NOAA		2 Oct 1992	Ongoing
KUM	Cape Kumukahi, USA	19.5	−154.8	0.02	–	NOAA	–	–
LEF	Park Falls, USA	45.9	−90.3	0.47	–	NOAA	–	–
MHD	Mace Head, Ireland	53.33	−9.9	0.01	NOAA/AGAGE	AGAGE <sup>b</sup>	3 Jun 1991	Ongoing
MLO	Mauna Loa, USA	19.54	−155.58	3.4	NOAA	NOAA	6 May 1983	Ongoing
NWR	Niwot Ridge, USA	40.05	−105.59	3.52	NOAA	NOAA	21 Jun 1983	Ongoing
PAL	Pallas-Sammaltunturi, Finland	67.97	24.12	0.56	NOAA		21 Dec 2001	Ongoing
PSA	Palmer Station, USA	−64.92	−64	0.01	NOAA	<sup>b</sup>	1 Jan 1983	Ongoing
RPB	Ragged Point, Barbados	13.17	−59.43	0.02	NOAA/AGAGE	AGAGE	14 Nov 1987	Ongoing
SEY	Mahe Island, Seychelles	−4.68	55.53	0	NOAA		12 May 1983	Ongoing
SMO	Tutuila, American Samoa	−14.25	−170.56	0.04	NOAA	NOAA/AGAGE	23 Apr 1983	Ongoing
SPO	South Pole, USA	−89.98	−24.8	2.81	NOAA	NOAA	20 Feb 1983	Ongoing
STM	Ocean Station M, Norway	66	2	0	NOAA		29 Apr 1983	27 Nov 2009
SUM	Summit, Greenland	72.6	−38.42	3.21	NOAA	<sup>b</sup>	23 Jun 1997	Ongoing
THD	Trinidad Head, USA	41.1	−124.1	0.1	AGAGE	AGAGE <sup>b</sup>	Sep 1995	Ongoing
ZEP	Ny-Ålesund, Norway	78.91	11.89	0.47	NOAA		11 Feb 1994	Ongoing

<sup>a</sup> For NOAA CH<sub>3</sub>CCl<sub>3</sub> data the record starts in 1992 at seven of the nine stations used here. It started in 1995 for KUM and 1996 for LEF. <sup>b</sup> NOAA flask data from these sites were not used in the present study or in Montzka et al. (2011).

Fig. 3 of Montzka et al., 2011) into yearly anomalies to produce relative interannual variations in the mean [OH]. Similarly, Rigby et al. (2013) used CH<sub>3</sub>CCl<sub>3</sub> measurements from on-site instrumentation operated continuously within the five-station AGAGE network in a 12-box model to produce yearly global [OH] anomalies from 1995 (the date from which data from all five stations are available) to 2010. These two time series, which convert anomalies in the CH<sub>3</sub>CCl<sub>3</sub> decay rate into anomalies in [OH] using constant temperature, correspond to the best estimate of [OH] variability from the two measurement networks by the groups who operate them. We then applied these two series of yearly global anomalies uniformly to the global latitude–height [OH] field used in the recent Atmospheric Tracer Transport Model Intercomparison Project (TransCom) CH<sub>4</sub> model intercomparison (see Patra et al., 2011), which itself was derived from a combination of semi-empirically calculated tropospheric OH distributions (Spivakovsky et al., 2000; Huijnen et al., 2010) and 2-D-model-simulated stratospheric loss rates (Velders, 1995). For consistency between the model experiments, both sets of yearly anomalies were scaled so that the mean [OH] between 1997 and 2007 (the overlap period where NOAA and AGAGE anomalies are both available) equalled the TransCom [OH] value. In the rest of this paper we refer to these two OH datasets as “NOAA-derived” and “AGAGE-derived”.

These two calculations of yearly [OH] anomalies use slightly different assumptions for CH<sub>3</sub>CCl<sub>3</sub> emissions after 2002. Before that year they use values from Prinn et al. (2005). The NOAA data then assumed a 20 % decay in emission for each subsequent year (Montzka et al.,

2011), while AGAGE used United Nations Environment Programme (UNEP) consumption values (UNEP, 2015). Holmes et al. (2013) suggested that inconsistencies in CH<sub>3</sub>CCl<sub>3</sub> observations between the AGAGE and NOAA networks also limit understanding of OH anomalies for specific years due to an unexplained phasing difference of up to around 3 months. As we are interested in the impact of [OH] changes over longer time periods (e.g. 2000–2006), this phase difference will be less important. We have investigated the impact of the different CH<sub>3</sub>CCl<sub>3</sub> observations and assumed emissions on the derived [OH] anomalies (see Sect. 3.1).

## 2.2 TOMCAT 3-D chemical transport model

We have used the TOMCAT global atmospheric 3-D off-line CTM (Chipperfield, 2006) to model atmospheric CH<sub>4</sub> and CH<sub>3</sub>CCl<sub>3</sub> concentrations. The TOMCAT simulations were forced by winds and temperatures from the 6-hourly European Centre for Medium-Range Weather Forecasts (ECMWF) ERA-Interim reanalyses (Dee et al., 2011). They covered the period 1993 to 2011 with a horizontal resolution of 2.8° × 2.8° and 60 levels from the surface to ~ 60 km.

The TOMCAT simulations use annually repeating CH<sub>4</sub> emissions, which have been scaled to previous estimates of 553 Tg yr<sup>−1</sup> (Ciais et al., 2013), taken from various studies (Fiore et al., 2006; Curry, 2007; Bergamaschi et al., 2009; Pison et al., 2009; Spahni et al., 2011; Ito and Inatomi, 2012). Annually repeating anthropogenic emissions (except biomass burning) were calculated from averaging the EDGAR v3.2 (2009) inventory from 1993 to 2009 (Olivier and Berowski, 2001). Biomass burning emissions were cal-

**Table 2.** Summary of the fifteen TOMCAT 3-D CTM simulations.

Run	OH time variation	Meteorology <sup>b</sup>	
		Winds <sup>c</sup>	Temperature <sup>d</sup>
RE_FTFW	Repeating <sup>a</sup>	Fixed	Fixed
RE_FTVW	Repeating <sup>a</sup>	Varying	Fixed
RE_VTVW	Repeating <sup>a</sup>	Varying	Varying
AP_FTFW	AGAGE (Rigby et al., 2013)	Fixed	Fixed
AP_FTVW	AGAGE (Rigby et al., 2013)	Varying	Fixed
AP_VTVW	AGAGE (Rigby et al., 2013)	Varying	Varying
AL_FTVT	AGAGE (this work)	Fixed	Fixed
AL_FTVW	AGAGE (this work)	Varying	Fixed
AL_VTVW	AGAGE (this work)	Varying	Varying
NP_FTFW	NOAA (Montzka et al., 2011)	Fixed	Fixed
NP_FTVW	NOAA (Montzka et al., 2011)	Varying	Fixed
NP_VTVW	NOAA (Montzka et al., 2011)	Varying	Varying
NL_FTFW	NOAA (this work)	Fixed	Fixed
NL_FTVW	NOAA (this work)	Varying	Fixed
NL_VTVW	NOAA (this work)	Varying	Varying

<sup>a</sup> Annually repeating [OH] taken from Patra et al. (2011). <sup>b</sup> Varying winds and temperatures are from ERA-Interim. <sup>c</sup> Fixed winds using repeating ERA-Interim winds from 1996. <sup>d</sup> Fixed temperatures use zonal mean ERA-Interim temperatures averaged over 1993–2009.

culated using the Global Fire Emissions Database (GFED) v3.1 inventory and averaged from 1997 to 2009 (van der Werf et al., 2010). The Joint UK Land Environment Simulator (JULES) (Best et al., 2011; Clark et al., 2011; Hayman et al., 2014) was used to calculate a wetland emission inventory between 1993 and 2009, which was then used to produce a mean annual cycle. Annually repeating rice (Yan et al., 2009), hydrate, mud volcano, termite, wild animal, and ocean (Matthews and Fung, 1987) emissions were taken from the TransCom CH<sub>4</sub> study (Patra et al., 2011). The methane loss fields comprised an annually repeating soil sink (Patra et al., 2011), an annually repeating stratospheric loss field (Velders, 1995), and a specified zonal mean [OH] field. This does not account for longitudinal variations in [OH], which are considered to be negligible compared to latitudinal variations. To create a reasonable spatial distribution, the model was spun up for 15 years prior to initialising the simulations, using emission data from 1977 to 1992 where available and annual averages otherwise. Before reinitialising the model in 1993, concentrations were scaled using the model and observed global concentrations to remove any imbalance.

Fifteen TOMCAT simulations were performed, each with a CH<sub>4</sub> tracer and a CH<sub>3</sub>CCl<sub>3</sub> tracer. The runs had differing treatments of meteorology (winds and temperature) and [OH] (see Table 2). Simulations with repeating [OH] fields (RE\_XXXX) used the TransCom dataset. The other runs with varying [OH] used the NOAA-derived or AGAGE-derived [OH] fields based on the original published work or our estimates (see Sect. 3.1). For these runs, the mean [OH] field is used where the respective NOAA or AGAGE-derived [OH] is unavailable or uncertain (before 1997/after 2007 for NOAA and before 1997/after 2009 for AGAGE). The five simulations with fixed wind and temperature fields (with labels ending in FTFW) used the ERA-Interim anal-

yses from 1996 repeated for all years. The five simulations with varying winds and fixed temperature (with labels ending in FTVW) used zonal mean temperature fields averaged from 1993 to 2009; any influence from the relatively small longitudinal temperature variations is unlikely to have a noticeable impact. We also derive our own [OH] anomalies from the anomaly in the CH<sub>3</sub>CCl<sub>3</sub> loss rate, which combines variations in atmospheric OH concentration with variations in temperature which affect the rate constant of the CH<sub>3</sub>CCl<sub>3</sub> + OH reaction. To quantify the importance of this temperature effect, we also performed five model runs which allow both winds and temperature to vary interannually according to ERA-Interim data (labels ending VTVW). Fixed-temperature simulations are used for general analysis because the derived OH anomalies already implicitly contain temperature variations.

### 3 Results

#### 3.1 Correlation of CH<sub>4</sub> variations with OH and temperature

We first investigate the extent to which variations in the observed CH<sub>4</sub> growth rate correlate with variations in derived [OH]. Figure 1a shows the published NOAA-derived and AGAGE-derived global [OH] anomalies along with the annual CH<sub>4</sub> growth rate estimated from the NOAA and AGAGE measurements. The two [OH] series show the similar behaviour of negative anomalies around 1997 and 2006–2007, and an extended period of more positive anomalies in between. For the time periods covered by the NOAA (1997–2007) and AGAGE (1997–2009) CH<sub>3</sub>CCl<sub>3</sub> observations, the two derived [OH] time series show negative correlations with the CH<sub>4</sub> growth from NOAA (regression coefficient,  $R = -0.32$ ) and AGAGE ( $R = -0.64$ ). Only the AGAGE [OH] correlation, from the longer time series, is statistically significant at the 90 % level. We assume that this correlation arises from variability in [OH] driving variability in CH<sub>4</sub> growth, although the correlation could be the result of a bidirectional effect, whereby decreased also CH<sub>4</sub> acts to increase [OH]. We note that Spivakovsky et al. (2000) showed a 25 % ( $\sim 450$  ppb) change in model CH<sub>4</sub> equates to a 5–6 % change in [OH]. This far exceeds the annual growth observed; therefore this effect is likely to be small. However, the concentration of other species which affect OH such as CO and volatile organic compounds (VOCs) can co-vary with the methane concentration, for example during years with high biomass burning emissions, so the effect may be larger than suggested by the Spivakovsky et al. (2000) study.

We can use a simple “global box model” (see Supplement Sect. S1) to estimate the [OH] variations required to fit the observed CH<sub>4</sub> growth rate variations, assuming constant CH<sub>4</sub> emissions and temperature (black line in Fig. 1b). This provides a crude guide to the magnitude of OH vari-

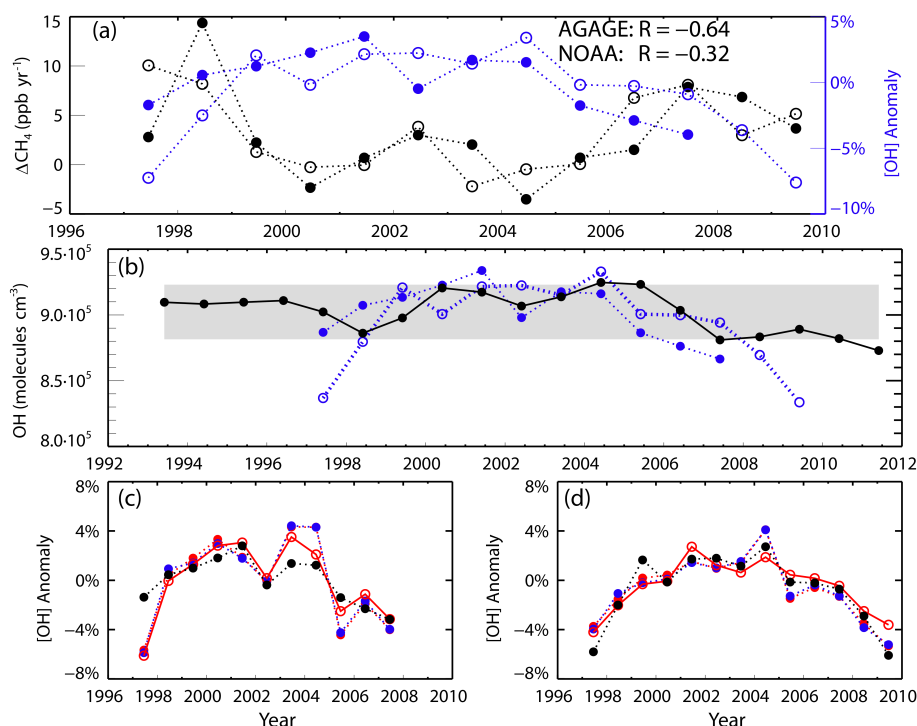


**Figure 1.** (a) Annual global CH<sub>4</sub> growth rate (ppb yr<sup>-1</sup>) derived from NOAA (filled black circles) and AGAGE (open black circles) data (left-hand y axis), and published annual global [OH] anomalies derived from NOAA (filled blue circles, 1997–2007) and AGAGE (open blue circles, 1997–2009) CH<sub>3</sub>CCl<sub>3</sub> measurements (right-hand y axis) (see text). (b) Annual mean [OH] (molecules cm<sup>-3</sup>) required for global box model (see Supplement Sect. S1) to fit yearly variations in NOAA CH<sub>4</sub> observations, assuming constant emissions and temperature ( $E = 553 \text{ Tg yr}^{-1}$ ;  $T = 272.9 \text{ K}$ ), based on Montzka et al. (2011) (solid black line). The shaded region denotes [OH] deviation of  $\pm 2.3 \%$  from the 1993–2011 mean. Also shown are the NOAA- and AGAGE-derived anomalies from panel (a) for an assumed mean OH (see Sect. 2.1). (c) Our estimates of [OH] derived from NOAA CH<sub>3</sub>CCl<sub>3</sub> calculated using a global box model (Supplement Sect. S1) using repeating (blue) and varying (red) annual mean temperature and the CH<sub>3</sub>CCl<sub>3</sub> emission scenario from UNEP (2015) (filled circles and dashed lines). Also shown for varying temperatures are results using the emissions of Montzka et al. (2011) (red open circles and solid line) based on Prinn et al. (2005) and the NOAA-derived values from panel (a) (black dashed line and circles). (d) As panel (c) but for OH derived from AGAGE CH<sub>3</sub>CCl<sub>3</sub> observations.

ations which could be important for changes in the CH<sub>4</sub> budget. Our results are consistent with those of Montzka et al. (2011), who performed a similar analysis on the NOAA CH<sub>4</sub> data. The required [OH] rarely exceeds their CH<sub>3</sub>CCl<sub>3</sub>-derived IAV range of [OH] ( $\pm 2.3 \%$ , shown as shading in the figure). Also shown in Fig. 1b are the published estimates of the global mean OH anomalies from Fig. 1a, converted to concentration units (see Sect. 2.1). The relative interannual variations in [OH] required to fit the CH<sub>4</sub> observations match the CH<sub>3</sub>CCl<sub>3</sub>-derived [OH] variations in many years, for example 1998–2002 (see Montzka et al., 2011). Some of the derived variations in [OH] exceed that required to match the CH<sub>4</sub> growth rate, with larger negative anomalies in the early and later years and some slightly larger positive values in the middle of the period.

Figure 1c and d show our estimates of [OH] using NOAA and AGAGE observations and two assumptions of post-2000 CH<sub>3</sub>CCl<sub>3</sub> emissions (see Sect. 2.1) in a global box model. The figures also compare our OH estimates with the NOAA-

derived and AGAGE-derived [OH] anomalies based on the work of the observation groups (Fig. 1a). Our results demonstrate the small impact of using different observations and post-2000 emission assumptions (compare filled and open red circles for the two panels). For these box model results there is also only a very small effect of using annually varying temperature (compare red and blue lines). In later years the choice of observations has a bigger impact than the choice of emissions on the derived [OH]. For AGAGE-derived values (Fig. 1d) our estimates agree well with the published values of Rigby et al. (2013), despite the fact we use a global box model while they used a more sophisticated 12-box model. In contrast, there are larger differences between our values and the NOAA-derived OH variability published by Montzka et al. (2011) (Fig. 1c), despite both studies using box models. In particular, around 2002–2003 we overestimate the positive anomaly in [OH]. We also estimate a much more negative OH anomaly in 1997 than Montzka et al. (2011), though we slightly underesti-

mate the published AGAGE-derived anomaly in that year (Fig. 1d). Tests show that differences between our results and the NOAA box model are due to the treatment of emissions. This suggests a larger uncertainty in the inferred low 1997 [OH] value, when emissions of CH<sub>3</sub>CCl<sub>3</sub> were decreasing rapidly, although reasons why atmospheric [OH] might have been anomalously low were discussed by Prinn et al. (2005). In the subsequent analysis we use the OH variability from the published NOAA and AGAGE studies as input to the 3-D model.

### 3.2 TOMCAT simulations

Overall, Fig. 1 shows the potential importance of small, observationally derived variations in OH concentrations to impact methane growth. We now investigate this quantitatively in the framework of a 3-D CTM.

#### 3.2.1 Methyl chloroform

The TOMCAT simulations include a CH<sub>3</sub>CCl<sub>3</sub> tracer. This allows us to verify that our approach of using a global OH field, scaled by derived anomalies, allows the model to reproduce the observed magnitude and variability of CH<sub>3</sub>CCl<sub>3</sub> decay accurately. Figure 2a shows that the model, with the imposed [OH] field, does indeed simulate the global decay of CH<sub>3</sub>CCl<sub>3</sub> very well. This justifies our use of the “offline” [OH] field, as models with interactive tropospheric chemistry can produce a large range in absolute global mean [OH] and therefore in lifetimes of gases such as CH<sub>3</sub>CCl<sub>3</sub>. For example, Voulgarakis et al. (2013) analysed the global mean [OH] from various 3-D models and found a range of  $0.65 \times 10^6$  to  $1.34 \times 10^6$  molecules cm<sup>-3</sup>. Furthermore, Montzka et al. (2011) discussed how photochemical models typically show smaller interannual variability than CH<sub>3</sub>CCl<sub>3</sub>-derived OH, again suggesting that the models are not accurately capturing all relevant processes. Figure 2a also shows that the global mean CH<sub>3</sub>CCl<sub>3</sub> from the NOAA and AGAGE networks differ by  $\sim 2.5$  ppt around 1993–1996, but since then this difference has become smaller.

The observed and modelled CH<sub>3</sub>CCl<sub>3</sub> decay rate anomalies (calculated using the method of Holmes et al. (2013) with a 12-month smoothing) are shown in Fig. 2b and c (different panels are used for AGAGE and NOAA comparisons for clarity). The model and observation-derived results both tend to show a faster CH<sub>3</sub>CCl<sub>3</sub> decay (more positive anomaly) in the middle of the period, with slower decay at the start and end. The anomalies for the NOAA- and AGAGE-derived OH show periodic variations on a timescale of 2–3 years but with a phase shift between the two datasets of 3 months, as noted by Holmes et al. (2013). The model runs with OH variability prescribed from the observations and varying winds also show these periodic variations with correlation coefficients ranging from 0.71 to 0.90. The correlation values for these runs using varying OH are all larger than the run

using repeating OH (for RE\_FTVW  $R = 0.62$  compared to AGAGE data and 0.67 compared to NOAA data). Note that for CH<sub>3</sub>CCl<sub>3</sub> decay there are only small differences between the 3-D simulations which use varying temperatures and the corresponding runs which use fixed temperature (e.g. simulation RE\_VTVW versus RE\_FTVW). This agrees with the results of Montzka et al. (2011) based on their box model. This shows that the largest contribution from the CH<sub>3</sub>CCl<sub>3</sub> decay rate anomaly comes from variations in atmospheric OH concentration, rather than atmospheric temperature. The simulations with repeating winds show less variability in the CH<sub>3</sub>CCl<sub>3</sub> decay rate, particularly in the period 1999–2004, but the small difference suggests that the interannual variability in the observed CH<sub>3</sub>CCl<sub>3</sub> decay rate is driven primarily by the variations in the OH concentration. The remaining interannual variability in run RE\_FTFW is due to variations in emissions.

Figure 3 shows the CH<sub>3</sub>CCl<sub>3</sub> decay and decay rate anomalies at four selected stations, two from the NOAA network and two from the AGAGE network. The good agreement in the global CH<sub>3</sub>CCl<sub>3</sub> decay in Fig. 2 is also seen at these individual stations. At the AGAGE stations of Mace Head and Cape Grim, the model runs with varying OH perform better in capturing the decay rate anomalies than the runs with repeating OH. However, the impact of variability in the winds (solid lines versus dotted lines) is more apparent at these individual stations compared to the global means. At the NOAA station of Mauna Loa the model run with varying OH and varying winds also appears to perform better in capturing the observed variability in CH<sub>3</sub>CCl<sub>3</sub> decay. At the South Pole the observed variability is small, except in 2000–2002. This feature is not captured by the model.

In summary, Figs. 2 and 3 show that the global OH fields that we have constructed from different datasets can perform well in capturing the decay of CH<sub>3</sub>CCl<sub>3</sub> and its anomalies both globally and at individual stations. Although the interannual variability in global mean OH has been derived from these CH<sub>3</sub>CCl<sub>3</sub> observations, the figures do show that the reconstructed model OH fields (which also depend on the methodology discussed in Sect. 2) perform well in simulating CH<sub>3</sub>CCl<sub>3</sub> within the 3-D model. Therefore, we would argue that these fields are suitable for testing the impact of OH variability on the methane growth rate. Even so, it is important to bear in mind that these fields may not represent the true changes in atmospheric OH, particularly if the interannual variability in CH<sub>3</sub>CCl<sub>3</sub> emissions was a lot different to that assumed here. However, we would again note that we are focussing on the impact of multi-year ( $\geq 2$  years) variability, which appears more robustly determined by the networks under differing assumptions of temperature and emissions than year-to-year variability.

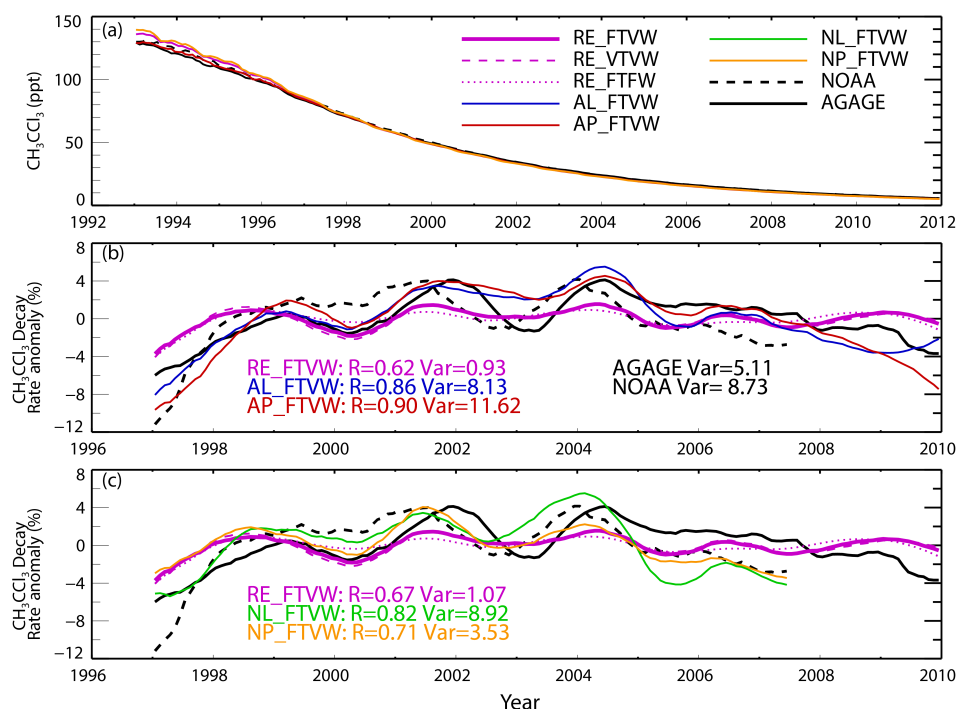


**Figure 2.** (a) Global mean surface CH<sub>3</sub>CCl<sub>3</sub> (ppt) from NOAA (black dashed) and AGAGE (black solid) observations from 1993 to 2012. Also shown are results from five TOMCAT simulations with fixed temperatures and varying winds (see Table 1). (b) Global surface CH<sub>3</sub>CCl<sub>3</sub> decay rate anomalies from NOAA and AGAGE along with model runs RE\_FTVW, AL\_FTVW, and AP\_FTVW (solid lines). Results from runs RE\_FTFW and RE\_VTVW are shown as a purple dotted line and dashed line, respectively. Observation and model anomalies are smoothed with a 12-month running average. Values given represent correlation coefficient when compared to AGAGE observations and variance. The decay rate anomaly is calculated from global mean CH<sub>3</sub>CCl<sub>3</sub> values using Eq. (1) from Holmes et al. (2013), expressed as a percentage of the typical decay with a 12-month smoothing. (c) As panel (b) but for model runs NL\_FTVW and NP\_FTVW, along with RE\_FTVW, RE\_VTVW, and RE\_FTFW, and correlation coefficients for comparison with NOAA observations. The model results are split across panels (b) and (c) for clarity.

### 3.2.2 Methane

Figure 4 shows deseasonalised modelled surface CH<sub>4</sub> from the 3-D CTM simulations compared with in situ observations from a northern high-latitude station (Alert), two tropical stations (Mauna Loa and Tutuila), a southern high-latitude station (South Pole), and the global average of the NOAA and AGAGE stations. The global comparisons are shown for simulations both with varying and repeating meteorology. Figure 5 shows the global annual CH<sub>4</sub> growth rates with a 12-month smoothing (panel a) and differences between the model and NOAA and AGAGE observations (panels b and c). The changes in the modelled global mean CH<sub>4</sub> over different time periods are given in Table 3.

Figure 4 shows that in 1993, at the end of the model spin-up, the simulations capture the global mean CH<sub>4</sub> level well, along with the observed values at a range of latitudes. The exception is at high northern latitudes. However, these differences are not important when investigating the change in the global growth rate. The global change in atmospheric CH<sub>4</sub> in all simulations from 1993 to the end of 2009 is between 75 and 104 ppb, compared to 56 and 66 ppb in the observations.

Model run RE\_FTFW does not include interannual variations in atmospheric transport or CH<sub>4</sub> loss. Therefore, and also given the lack of change in emissions, the modelled CH<sub>4</sub> gradually approaches a steady-state value of  $\sim 1830$  ppb (Fig. 4f). The rate of CH<sub>4</sub> growth decreases from  $7.9 \text{ ppb yr}^{-1}$  (1993–1998) to  $1.4 \text{ ppb yr}^{-1}$  (2007–2009). Compared to run RE\_FTFW, the other simulations introduce variability on this CH<sub>4</sub> evolution.

Run RE\_FTVW includes interannual variability in wind fields which may alter the transport of CH<sub>4</sub> from the source (emission) to the sink regions. The largest difference between runs RE\_FTFW and RE\_FTVW occurs after 2000 (Fig. 4f). During the stagnation period (1999–2006) run RE\_FTVW has a smaller growth rate of  $3.5 \text{ ppb yr}^{-1}$  compared to  $4.1 \text{ ppb yr}^{-1}$  in run RE\_FTFW, showing that variations in atmospheric transport made a small contribution to the slowdown in global mean CH<sub>4</sub> growth.

Compared to run RE\_FTVW, runs AP\_FTVW, AL\_FTVW, NP\_FTVW, and NL\_FTVW include CH<sub>3</sub>CCl<sub>3</sub>-derived interannual variations in [OH] which introduce large changes in modelled CH<sub>4</sub>, which are more in line



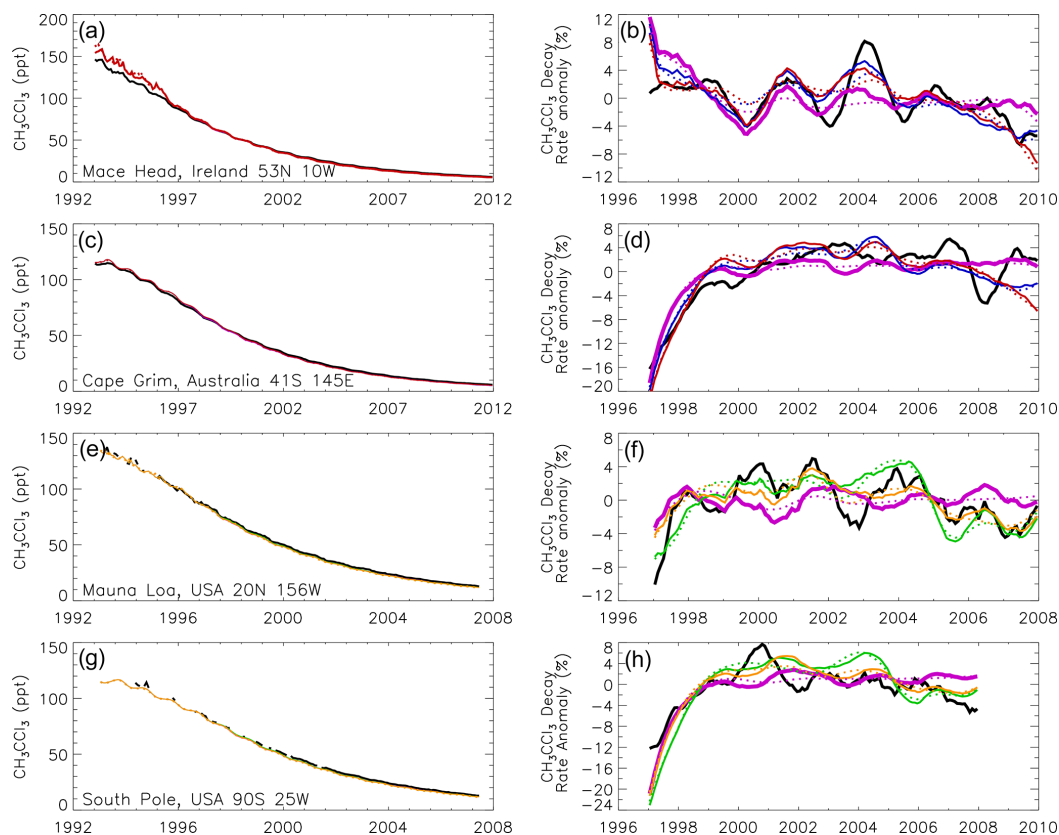


**Figure 3.** (Left) Observed mean surface CH<sub>3</sub>CCl<sub>3</sub> (ppt) (black line) from (a) Mace Head (AGAGE), (c) Cape Grim (AGAGE), (e) Mauna Loa (NOAA), and (g) South Pole (NOAA). Also shown are results from five TOMCAT simulations with fixed temperatures and varying winds (FTVW; for legend see Fig. 2a). (Right) Surface CH<sub>3</sub>CCl<sub>3</sub> decay rate anomalies at the same station as the corresponding left column plot for observations (black), TOMCAT simulations with varying winds (FTVW, solid coloured lines), and TOMCAT simulations with fixed winds (FTFW, dotted lines). Comparisons at NOAA (AGAGE) stations show only comparisons with runs using NOAA (AGAGE)-derived OH, along with runs RE\_FTVW and RE\_FTFW in all panels.

**Table 3.** Calculated methane changes over different time periods from selected TOMCAT experiments and the NOAA and AGAGE observation networks. Standard errors shown are calculated from statistically independent unsmoothed monthly global CH<sub>4</sub> growth data.

Model run or observation network	Global mean $\Delta\text{CH}_4$ in ppb ( $\text{ppb yr}^{-1}$ )			
	2009–1993	1998–1993	2006–1999	2009–2007
RE_FTFW	85.0 (5.0 ± 0.2)	47.2 (7.9 ± 0.1)	32.9 (4.1 ± 0.1)	4.3 (1.4 ± 0.1)
RE_FTVW	82.2 (4.8 ± 0.2)	48.2 (8.0 ± 0.3)	27.8 (3.5 ± 0.3)	5.4 (1.8 ± 0.3)
RE_VTVW	74.6 (4.4 ± 0.2)	45.6 (7.6 ± 0.2)	23.1 (2.9 ± 0.2)	5.3 (1.8 ± 0.2)
AP_FTVW <sup>a</sup>	97.7 <sup>c</sup> (5.7 ± 0.4)	62.3 <sup>c</sup> (10.4 ± 0.5)	8.2 <sup>g</sup> (1.0 ± 0.4)	26.4 (8.8 ± 0.6)
AL_FTVW <sup>b</sup>	104.2 <sup>c</sup> (6.1 ± 0.4)	58.4 <sup>c</sup> (9.7 ± 0.4)	17.3 (2.2 ± 0.5)	27.5 (9.2 ± 0.5)
NP_FTVW <sup>c</sup>	86.2 <sup>f</sup> (5.1 ± 0.3)	49.7 <sup>f</sup> (8.3 ± 0.3)	24.8 (3.1 ± 0.4)	10.6 <sup>f</sup> (3.8 ± 0.7)
NL_FTVW <sup>d</sup>	91.4 <sup>f</sup> (5.4 ± 0.5)	58.8 <sup>f</sup> (9.8 ± 0.5)	20.1 (2.5 ± 0.6)	11.3 <sup>f</sup> (3.8 ± 1.0)
NOAA obs.	56.1 (3.3 ± 0.3)	36.0 (6.0 ± 0.4)	4.8 (0.6 ± 0.3)	14.7 (4.9 ± 0.4)
AGAGE obs.	66.3 (3.9 ± 0.4)	42.6 (7.1 ± 0.9)	5.6 (0.7 ± 0.7)	17.4 (5.8 ± 0.7)

<sup>a</sup> Taken from Rigby et al. (2013) and Patra et al. (2011). <sup>b</sup> Using 1997–2009 relative annual changes in mean [OH] derived from AGAGE data (Cunnold et al., 2002). <sup>c</sup> Taken from Montzka et al. (2011) and Patra et al. (2011). <sup>d</sup> Using 1997–2007 relative annual changes in mean [OH] derived from NOAA data (Prinn et al., 2015). <sup>e</sup> Value using mean [OH] from 1993 to 1996. <sup>f</sup> Value using mean [OH] from 1993 to 1996 and 2008 to 2011. <sup>g</sup> Trend value not statistically significant at the 90 % level.



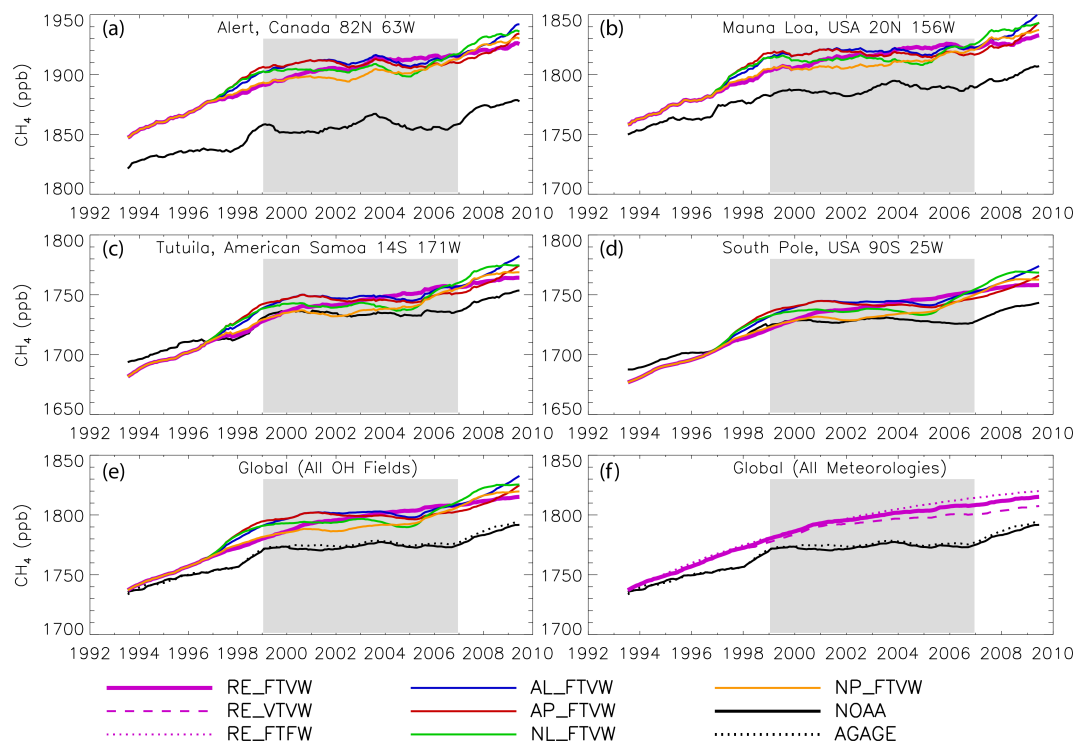


**Figure 4.** (a, b, c, d) Deseasonalised surface CH<sub>4</sub> (ppb) from four NOAA sites (black solid line) from 1993 to 2009. Also shown are results from five TOMCAT 3-D CTM simulations with fixed temperatures and varying winds (FTVW; see Table 2). (e) Deseasonalised global mean surface CH<sub>4</sub> from NOAA (black solid) and AGAGE (black dashed) observations along with five TOMCAT simulations with different treatments of OH. (f) Same as (e) but for TOMCAT simulations using repeating OH (RE) and different treatments of winds and temperature. All panels use observation and model values which are smoothed with a 12-month running average. The shaded region marks the stagnation period in the observed CH<sub>4</sub> growth rate.

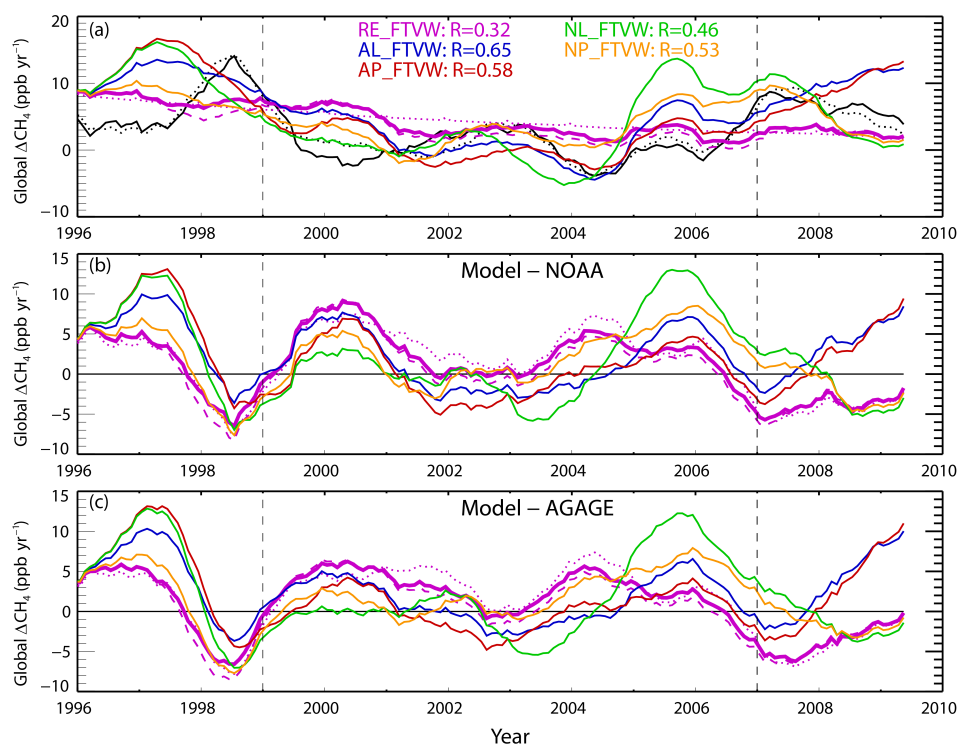
with the observations (Figs. 4e and 5). These runs produce turnarounds in the CH<sub>4</sub> growth in 2001–2002 (becomes negative) and 2005–2006 (returns to being positive). For AGAGE-derived [OH] (runs AP\_FTVW, AL\_FTVW) the large negative anomaly in OH in 1997 produces a significant increase in CH<sub>4</sub> prior to the turnaround in 2001.

Table 3 summarises the change in global mean CH<sub>4</sub> over different time periods. These periods are defined by the key dates in the observed record, i.e. 1999 and 2006 as the start and end dates of the stagnation period. Comparison of Fig. 4e and Table 3 shows, however, that the timing of the largest modelled change in growth rate does not necessarily coincide with those dates. That is understandable if other factors not considered here, e.g. emission changes, are contributing to the change in global CH<sub>4</sub> concentration. It does mean that the summary model values in Table 3 do not capture the full impact of the changes in [OH] and winds within the stagnation period. Figure 4e shows that model runs with varying OH perform better in simulating the relative CH<sub>4</sub> trend from 1999 to around 2004.

Table 3 shows that runs NP\_FTVW and NL\_FTVW (NOAA-derived [OH]) produce a small modelled CH<sub>4</sub> growth of 2.5–3.1 ppb yr<sup>−1</sup> during the stagnation period

(1999–2006), compared to 1.0 ppb yr<sup>−1</sup> for run AP\_FTVW (AGAGE-derived [OH]). The AGAGE results are slightly larger than the observed growth rate of 0.6–0.7 ppb yr<sup>−1</sup>. Runs AL\_FTVW, AP\_FTVW, NL\_FTVW, and NP\_FTVW capture the observed strong decrease in the CH<sub>4</sub> growth rate. With the exception of AP\_FTVW between 1999 and 2006 (*p* value = 0.37) all trends, over all three time periods, are statistically significant at the 90 % level. Clearly, these runs demonstrate the significant potential for relatively small variations in mean [OH] to affect CH<sub>4</sub> growth. Excluding the stagnation period, the mean modelled CH<sub>4</sub> lifetime in run NP\_FTVW is 9.4 years, but this decreases slightly by 0.01 years during the stagnation period. For run AP\_FTVW there is a decrease of 0.18 years from 9.6 years between the same intervals. The results from all the CTM simulations during 1999–2006 indicate that the accuracy of modelled CH<sub>4</sub> growth is improved by accounting for interannual variability in [OH] as derived from CH<sub>3</sub>CCl<sub>3</sub> observations and interannual variability in meteorology.

The variation of [OH] after 2007 cannot be determined from the available NOAA data, so run NP\_FTVW used the mean [OH] field for all subsequent years. The modelled CH<sub>4</sub> increase of 3.5 ppb yr<sup>−1</sup> underestimates the observa-



**Figure 5.** (a) The smoothed variation in the global annual CH<sub>4</sub> growth rate (ppb yr<sup>-1</sup>) derived from NOAA (black solid) and AGAGE (black dashed) observations. Also shown are the smoothed growth rates from five TOMCAT 3-D CTM simulations with fixed temperatures and varying winds (FTVW; see Table 1). Values in legend give correlation coefficient between model run and NOAA observations. Also shown are results from runs RE\_FTVW and RE\_VTVW as a purple dotted line and dashed line, respectively. (b) The difference in smoothed growth rate between TOMCAT simulations and NOAA observations shown in panel (a). (c) Same as (b) except using differences compared to AGAGE observations. The vertical dashed lines mark the start and end of the stagnation period in the observed CH<sub>4</sub> growth rate (1999–2006).

tions (4.9 ppb yr<sup>-1</sup>). Should the lower [OH] of 2007 have persisted, then the model would have produced a larger increase in CH<sub>4</sub>, in better agreement with the observations. The AGAGE-derived [OH] for 2007–2009 (run AP\_FTVW) produces a larger CH<sub>4</sub> growth relative to the previous years (8.8 ppb yr<sup>-1</sup>). Runs RE\_FTVW (1.4 ppb yr<sup>-1</sup>) and RE\_VTVW (1.8 ppb yr<sup>-1</sup>) both show a decreased rate of growth during the final 5 years, consistent with a system approaching steady state.

Figure 5a shows the global CH<sub>4</sub> growth rate derived from the AGAGE and NOAA networks together with selected model simulations. Figure 5b and c show the differences between the model simulations and the NOAA and AGAGE observations, respectively. The runs which include variations in [OH] agree better with the observed changes, i.e. larger *R* values in panel (a) and the model lines being closer to the *y* = 0 line in panels (b) and (c), especially in the first 5 years of the stagnation period. It is interesting to note that the relative impacts of wind and temperature variations are larger for CH<sub>4</sub> than for CH<sub>3</sub>CCl<sub>3</sub> (compare simulations RE\_FTVW, RE\_VTVW, and RE\_VTVW in Figs. 2 and 5a). The temperature dependences of the OH loss reactions are similar for the two species (see Supplement Sect. S1), but the impact

of variability in transport is likely to be greater for CH<sub>4</sub> due to its stronger spatial gradients than for CH<sub>3</sub>CCl<sub>3</sub>. Figure S2 in the Supplement shows the very weak horizontal gradients in CH<sub>3</sub>CCl<sub>3</sub> in its period of atmospheric decay due to small emissions. In contrast, variations in emissions lead to large spatial gradients in CH<sub>4</sub> which can then couple with variability in transport. This lack of spatial variability in CH<sub>3</sub>CCl<sub>3</sub> is an advantage when using this species to derive OH variability as it reduces the possible complication from transport variability. The impact of variability in temperature will remain, however. In principle, it would be possible to use a 3-D inverse model with realistic temperature fields to derive a time-dependent 3-D OH field which is consistent with the CH<sub>3</sub>CCl<sub>3</sub> decay. However, there are not enough observations to constrain such a model. Using the TOMCAT model, in Supplement S2 we test whether differences in the distribution of the CH<sub>3</sub>CCl<sub>3</sub> and CH<sub>4</sub> observation networks will affect the anomaly signal derived by the application of the same OH field. The results there show that the differences in the distribution of the observing stations are not likely to be important.

#### 4 Discussion and conclusions

Our model results suggest that variability in atmospheric [OH] played a key role in the observed recent variations in CH<sub>4</sub> growth, particularly during the CH<sub>4</sub> stagnation period between 1999 and 2006. The 3-D CTM calculations show that, during the stagnation period, variations in atmospheric conditions in the tropical lower to mid-troposphere could potentially account for an important component of the observed decrease in global CH<sub>4</sub> growth. Within this, small increases in [OH] were the largest factor, while variations in transport from source to sink regions made a smaller contribution. Note again, however, that the ultimate loss of CH<sub>4</sub> is still due to chemistry. The role of atmospheric temperature variations is factored into the observationally derived OH, but model experiments show that changes in the OH concentration itself is most important. The remainder of the variation can be ascribed to other processes not considered in our runs such as emission changes. There are also measurement uncertainties to consider and the possible underrepresentation of the global mean CH<sub>3</sub>CCl<sub>3</sub> which will affect the derived OH concentration. Our results are consistent with an earlier budget study which analysed 1991 to 2004 and found that variations in [OH] were the main control of variations in atmospheric CH<sub>4</sub> lifetime (65 %), with temperature accounting for a smaller fraction (35 %) (Fiore et al., 2006). However, they were not able to study the full period of the pause in CH<sub>4</sub> growth and did not impose observation-based [OH] variations. As we have noted here, the CH<sub>4</sub> lifetime can also be affected by emission distributions which affect transport to the main loss regions.

Prior to the stagnation period the simulation using AGAGE-derived [OH] (9.7–10.4 ppb yr<sup>-1</sup>) overestimates CH<sub>4</sub> growth when compared to observations (6.0–7.1 ppb yr<sup>-1</sup>), which degrades the agreement with the observed CH<sub>4</sub> variations. A likely cause of this is inaccuracies in derived [OH] in 1997, when emissions still played a large role in the observed CH<sub>3</sub>CCl<sub>3</sub> and the *e*-fold decay had not yet stabilised (Montzka et al., 2011).

We have not accounted for expected variations in CH<sub>4</sub> emissions in this study. We can conclude that although global CH<sub>4</sub> emissions do vary year to year, the observed trend in CH<sub>4</sub> growth between 1999 and 2006 was impacted by changing atmospheric processes that affected CH<sub>4</sub> loss. Changes in emissions are still important over this time period and likely still dominate CH<sub>4</sub> variations over other time periods. The observed changes in growth rates during ENSO events in e.g. 1998 are poorly captured by the meteorological changes considered here and can be attributed to changes in emissions through changing precipitation and enhanced biomass burning (Hodson et al., 2011). The renewed growth of CH<sub>4</sub> in 2007 is also poorly captured by all model simulations without varying [OH]. The observed decrease in AGAGE- and NOAA-derived [OH] coincides with the increase in CH<sub>4</sub> growth in 2007, although the currently available data do not

allow for a more detailed investigation of the possible contribution of [OH] changes in this recent increase.

Despite the differences in year-to-year variability in [OH] derived from CH<sub>3</sub>CCl<sub>3</sub> observations (Holmes et al., 2013), we find that [OH] variability derived from two different networks of surface CH<sub>3</sub>CCl<sub>3</sub> observations over multi-year periods provide insights into atmospheric CH<sub>4</sub> variations. Improved quantification of the role of OH variability will require efforts to reduce uncertainties associated with estimating [OH]. Estimates of global mean [OH] in recent years from CH<sub>3</sub>CCl<sub>3</sub> observations are becoming increasingly difficult because CH<sub>3</sub>CCl<sub>3</sub> levels are currently < 5 ppt; hence this may limit the accuracy of derived [OH] and its variability in future years (Lelieveld et al., 2006). Wennberg et al. (2004) also noted that there can be time variations in the net flux of CH<sub>3</sub>CCl<sub>3</sub> by the oceans, which could potentially affect the derived [OH] concentrations and which were not considered in our analysis. However, the impact of interannual variability in this flux is not likely to be important. For the period considered in this study, Fig. 2 of Wennberg et al. (2004) shows that the CH<sub>3</sub>CCl<sub>3</sub> flux into the ocean decreased from the largest value in 1997 to almost zero in recent years, which mimics CH<sub>3</sub>CCl<sub>3</sub> emissions. Including the estimated 1997 ocean flux in our box model decreased the OH anomaly for that year by 0.8 %. This change would decrease in magnitude in the subsequent years. Overall, accurate estimates of [OH] beyond 2009 will require more sophisticated analysis of CH<sub>3</sub>CCl<sub>3</sub> observations, derivation from other species, or improved representation of [OH] in photochemical models.

Overall our study suggests that future atmospheric trends in CH<sub>4</sub> are likely to be strongly influenced not only by emissions but also by changes in processes that affect atmospheric loss. Therefore, to be realistic, predictions of these future trends need to explicitly account for likely variations in [OH], the major sink, and possibly other processes related to tropospheric and stratospheric chemistry.

#### 5 Data availability

The observational data used in this paper are available at: <http://www.esrl.noaa.gov/gmd/dv/data> (NOAA data) <http://cdiac.esd.ornl.gov/ndps/alegage.html> (AGAGE data).

Model data are available on request, please contact: [ee-jrm@leeds.ac.uk](mailto:ee-jrm@leeds.ac.uk) or [m.chipperfield@leeds.ac.uk](mailto:m.chipperfield@leeds.ac.uk)

**The Supplement related to this article is available online at doi:10.5194/acp-16-7943-2016-supplement.**

**Acknowledgements.** J. McNorton thanks NERC National Centre for Earth Observation (NCEO) for a studentship. C. Wilson, M. P. Chipperfield and M. Gloor acknowledge support from NERC grants GAUGE (NE/K002244/1) and AMAZONICA (NE/F005806/1). G. D. Hayman acknowledges support from the European Space Agency through its Support to Science Element initiative (ALANIS Methane), NCEO, and the NERC MAMM grant (NE/I028327/1). S. A. Montzka acknowledges support in part from NOAA Climate Program Office's AC4 programme. AGAGE is supported by NASA grants NNX11AF17G to MIT and NNX11AF15G and NNX11AF16G to SIO, by NOAA, by UK Department of Food and Rural Affairs (DEFRA) and UK Department for Energy and Climate Change (DECC) grants to Bristol University, and by CSIRO and Australian Bureau of Meteorology. M. Rigby is supported by a NERC Advanced Fellowship (NE/I021365/1). Model calculations were performed on the Arc1 and Archer supercomputers.

Edited by: B. N. Duncan

## References

- Bergamaschi, P., Frankenberg, C., Meirink, J. F., Krol, M., Vilani, M. G., Houweling, S., Dentener, F., Dlugokencky, E. J., Miller, J. B., Gatti, L. V., Engel, A., and Levin, I.: Inverse modeling of global and regional CH<sub>4</sub> emissions using SCIAMACHY satellite retrievals, *J. Geophys. Res.*, 114, D22301, doi:10.1029/2009jd012287, 2009.
- Best, M. J., Pryor, M., Clark, D. B., Rooney, G. G., Essery, R. L. H., Ménard, C. B., Edwards, J. M., Hendry, M. A., Porson, A., Gedney, N., Mercado, L. M., Sitch, S., Blyth, E., Boucher, O., Cox, P. M., Grimmond, C. S. B., and Harding, R. J.: The Joint UK Land Environment Simulator (JULES), model description – Part 1: Energy and water fluxes, *Geosci. Model Dev.*, 4, 677–699, doi:10.5194/gmd-4-677-2011, 2011.
- Bousquet, P., Ciais, P., Miller, J. B., Dlugokencky, E. J., Hauglustaine, D. A., Prigent, C., Van der Werf, G. R., Peylin, P., Brunke, E. G., Carouge, C., Langenfelds, R. L., Lathiere, J., Papa, F., Ramonet, M., Schmidt, M., Steele, L. P., Tyler, S. C., and White, J.: Contribution of anthropogenic and natural sources to atmospheric methane variability, *Nature*, 443, 439–443, doi:10.1038/nature05132, 2006.
- Bousquet, P., Ringeval, B., Pison, I., Dlugokencky, E. J., Brunke, E. G., Carouge, C., Chevallier, F., Fortems-Cheiney, A., Frankenberg, C., Hauglustaine, D. A., Krummel, P. B., Langenfelds, R. L., Ramonet, M., Schmidt, M., Steele, L. P., Szopa, S., Yver, C., Viovy, N., and Ciais, P.: Source attribution of the changes in atmospheric methane for 2006–2008, *Atmos. Chem. Phys.*, 11, 3689–3700, doi:10.5194/acp-11-3689-2011, 2011.
- Chipperfield, M. P.: New version of the TOMCAT/SILMCAT offline chemical transport model: Intercomparison of stratospheric tracer experiments, *Q. J. Roy. Meteor. Soc.*, 132, 1179–1203, 2006.
- Ciais, P., Sabine, C., Bala, G., Bopp, L., Brovkin, V., Canadell, J., Chhabra, A., DeFries, R., Galloway, J., Heimann, M., Jones, C., Le Quere, C., Myneni, R. B., Piao, S., and Thornton, P.: Carbon and other biogeochemical cycles, in: *Climate Change 2013: The Physical Science Basis. Contribution of Working Group I to the Fifth Assessment Report of the Intergovernmental Panel on Climate Change*, Cambridge University Press, 2013.
- Cicerone, R. J. and Oremland, R. S.: Biogeochemical aspects of atmospheric methane, *Global Biogeochem. Cy.*, 2, 299–327, 1988.
- Clark, D. B., Mercado, L. M., Sitch, S., Jones, C. D., Gedney, N., Best, M. J., Pryor, M., Rooney, G. G., Essery, R. L. H., Blyth, E., Boucher, O., Harding, R. J., Huntingford, C., and Cox, P. M.: The Joint UK Land Environment Simulator (JULES), model description – Part 2: Carbon fluxes and vegetation dynamics, *Geosci. Model Dev.*, 4, 701–722, doi:10.5194/gmd-4-701-2011, 2011.
- Cunnold, D., Steele, L., Fraser, P., Simmonds, P., Prinn, R., Weiss, R., Porter, L., O'Doherty, S., Langenfelds, R., and Krummel, P.: In situ measurements of atmospheric methane at GAGE/AGAGE sites during 1985–2000 and resulting source inferences, *J. Geophys. Res.*, 107, ACH 20-21-ACH 20-18, doi:10.1029/2001JD001226, 2002.
- Curry, C. L.: Modeling the soil consumption of atmospheric methane at the global scale, *Global Biogeochem. Cy.*, 21, GB4012, doi:10.1029/2006GB002818, 2007.
- Dee, D. P., Uppala, S. M., Simmons, A. J., Berrisford, P., Poli, P., Kobayashi, S., Andrae, U., Balmaseda, M. A., Balsamo, G., Bauer, P., Bechtold, P., Beljaars, A., van de Berg, L., Bidlot, J., Bormann, N., Delsol, C., Dragani, R., Fuentes, M., Geer, A. J., Haimberger, L., Healy, S. B., Hersbach, H., Hölm, E. V., Isaksen, I., Kallberg, P., Köhler, M., Matricardi, M., McNally, A. P., Monge-Sanz, B. M., Morcrette, J.-J., Park, B. K., Peubey, C., de Rosnay, P., Tavolato, C., Thépaut, J.-N., and Vitart, F.: The ERA-Interim reanalysis: Configuration and performance of the data assimilation system, *Q. J. Roy. Meteor. Soc.*, 137, 553–597, 2011.
- Dlugokencky, E. J., Houweling, S., Bruhwiler, L., Masarie, K., Lang, P., Miller, J., and Tans, P.: Atmospheric methane levels off: Temporary pause or a new steady-state?, *Geophys. Res. Lett.*, 30, 19, doi:10.1029/2003GL018126, 2003.
- Dlugokencky, E. J., Myers, R., Lang, P., Masarie, K., Crotwell, A., Thoning, K., Hall, B., Elkins, J., and Steele, L.: Conversion of NOAA atmospheric dry air CH<sub>4</sub> mole fractions to a gravimetrically prepared standard scale, *J. Geophys. Res.*, 110, D18306, doi:10.1029/2005JD006035, 2005.
- Dlugokencky, E. J., Nisbet, E. G., Fisher, R., and Lowry, D.: Global atmospheric methane: budget, changes and dangers, *Philos. Trans. R. Soc. A*, 369, 2058–2072, doi:10.1098/rsta.2010.0341, 2011.
- Dlugokencky, E. J., Lang, P. M., Crotwell, A. M., Masarie, K. A., and Crotwell, M. J.: Atmospheric Methane Dry Air Mole Fractions from the NOAA ESRL Carbon Cycle Cooperative Global Air Sampling Network, 1983–2013, Version: 2014-06-24, available at: [ftp://ftp.cmdl.noaa.gov/data/trace\\_gases/ch4/flask/surface/](ftp://ftp.cmdl.noaa.gov/data/trace_gases/ch4/flask/surface/), last access: 6 July 2014.
- Etheridge, D. M., Steele, L. P., Francey, R. J., and Langenfelds, R. L.: Atmospheric methane between 1000 A.D. and present: Evidence of anthropogenic emissions and climatic variability, *J. Geophys. Res.*, 103, 15979–15993, doi:10.1029/98jd00923, 1998.
- Fiore, A. M., Horowitz, L. W., Dlugokencky, E. J., and West, J. J.: Impact of meteorology and emissions on methane trends, 1990–2004, *Geophys. Res. Lett.*, 33, L12809, doi:10.1029/2006gl026199, 2006.

- Hayman, G. D., O'Connor, F. M., Dalvi, M., Clark, D. B., Gedney, N., Huntingford, C., Prigent, C., Buchwitz, M., Schneising, O., Burrows, J. P., Wilson, C., Richards, N., and Chipperfield, M.: Comparison of the HadGEM2 climate-chemistry model against in situ and SCIAMACHY atmospheric methane data, *Atmos. Chem. Phys.*, 14, 13257–13280, doi:10.5194/acp-14-13257-2014, 2014.
- Hodson, E. L., Poulter, B., Zimmermann, N. E., Prigent, C., and Kaplan, J. O.: The El Niño–Southern Oscillation and wetland methane interannual variability, *Geophys. Res. Lett.*, 38, L08810, doi:10.1029/2011gl046861, 2011.
- Holmes, C. D., Prather, M. J., Søvde, O. A., and Myhre, G.: Future methane, hydroxyl, and their uncertainties: key climate and emission parameters for future predictions, *Atmos. Chem. Phys.*, 13, 285–302, doi:10.5194/acp-13-285-2013, 2013.
- Huijnen, V., Williams, J., van Weele, M., van Noije, T., Krol, M., Dentener, F., Segers, A., Houweling, S., Peters, W., de Laat, J., Boersma, F., Bergamaschi, P., van Velthoven, P., Le Sager, P., Eskes, H., Alkemade, F., Scheele, R., Nédélec, P., and Pätz, H.-W.: The global chemistry transport model TM5: description and evaluation of the tropospheric chemistry version 3.0, *Geosci. Model Dev.*, 3, 445–473, doi:10.5194/gmd-3-445-2010, 2010.
- Ito, A. and Inatomi, M.: Use of a process-based model for assessing the methane budgets of global terrestrial ecosystems and evaluation of uncertainty, *Biogeosciences*, 9, 759–773, doi:10.5194/bg-9-759-2012, 2012.
- Karlsdotir, S. and Isaksen, I. S. A.: Changing methane lifetime: Possible cause for reduced growth, *Geophys. Res. Lett.*, 27, 93–96, 2000.
- Kirschke, S., Bousquet, P., Ciais, P., Saunio, M., Canadell, J. G., Dlugokencky, E. J., Bergamaschi, P., Bergmann, D., Blake, D. R., Bruhwiler, L., Cameron-Smith, P., Castaldi, S., Chevallier, F., Feng, L., Fraser, A., Heimann, M., Hodson, E. L., Houweling, S., Josse, B., Fraser, P. J., Krummel, P. B., Lamarque, J.-F., Langenfelds, R. L., Le Quere, C., Naik, V., O'Doherty, S., Palmer, P. I., Pison, I., Plummer, D., Poulter, B., Prinn, R. G., Rigby, M., Ringeval, B., Santini, M., Schmidt, M., Shindell, D. T., Simpson, I. J., Spahni, R., Steele, L. P., Strode, S. A., Sudo, K., Szopa, S., van der Werf, G. R., Voulgarakis, A., van Weele, M., Weiss, R. F., Williams, J. E., and Zeng, G.: Three decades of global methane sources and sinks, *Nat. Geosci.*, 6, 813–823, 2013.
- Lelieveld, J., Dentener, F. J., Peters, W., and Krol, M. C.: On the role of hydroxyl radicals in the self-cleansing capacity of the troposphere, *Atmos. Chem. Phys.*, 4, 2337–2344, doi:10.5194/acp-4-2337-2004, 2004.
- Lelieveld, J., Brenninkmeijer, C. A. M., Joeckel, P., Isaksen, I. S. A., Krol, M. C., Mak, J. E., Dlugokencky, E., Montzka, S. A., Novelli, P. C., Peters, W., and Tans, P. P.: New Directions: Watching over tropospheric hydroxyl (OH), *Atmos. Environ.*, 40, 5741–5743, 2006.
- Matthews, E. and Fung, I.: Methane emissions from natural wetlands: Global distribution, area, and ecology of sources, *Global Biogeochem. Cy.*, 1, 61–86, 1987.
- Montzka, S. A., Krol, M., Dlugokencky, E., Hall, B., Jöckel, P., and Lelieveld, J.: Small interannual variability of global atmospheric hydroxyl, *Science*, 331, 67–69, 2011.
- Myhre, G., Shindell, D., Bréon, F., Collins, W., Fuglestad, J., Huang, J., Koch, D., Lamarque, J., Lee, D., Mendoza, B., Nakajima, T., Robock, A., Stephens, G., Takemura, T., and Zhang, H.: Anthropogenic and natural radiative forcing, in: *Climate Change 2013: The Physical Science Basis. Contribution of Working Group I to the Fifth Assessment Report of the Intergovernmental Panel on Climate Change*, Cambridge University Press, 2013.
- Nisbet, E. G., Dlugokencky, E. J., and Bousquet, P.: Atmospheric science, Methane on the rise – again, *Science*, 343, 493–495, doi:10.1126/science.1247828, 2014.
- Olivier, J. G. and Berdowski, J. J. M.: Global emissions sources and sinks, in: *The Climate System*, edited by: Berdowski, J., Guicherit, R., and Heij, B. J., IISBN 9058092550, A. A. Balkema Publishers/Swets & Zeitlinger Pub., Lisse, The Netherlands, 33–78, 2001.
- Olivier, J. G., Van Aardenne, J. A., Dentener, F. J., Pagliari, V., Ganzeveld, L. N., and Peters, J. A.: Recent trends in global greenhouse gas emissions: regional trends 1970–2000 and spatial distribution of key sources in 2000, *Environ. Sci.*, 2, 81–99, 2005.
- Patra, P. K., Takigawa, M., Ishijima, K., Choi, B.-C., Cunnold, D., J. Dlugokencky, E., Fraser, P., J. Gomez-Pelaez, A., Goo, T.-Y., Kim, J.-S., Krummel, P., Langenfelds, R., Meinhardt, F., Mukai, H., O'Doherty, S., G. Prinn, R., Simmonds, P., Steele, P., Tohjima, Y., Tsuboi, K., Uhse, K., Weiss, R., Worthly, D., and Nakazawa, T.: Growth rate, seasonal, synoptic, diurnal variations and budget of methane in the lower atmosphere, *J. Meteorol. Soc. Jpn.*, 87, 635–663, doi:10.2151/jmsj.87.635, 2009.
- Patra, P. K., Houweling, S., Krol, M., Bousquet, P., Belikov, D., Bergmann, D., Bian, H., Cameron-Smith, P., Chipperfield, M. P., Corbin, K., Fortems-Cheiney, A., Fraser, A., Gloor, E., Hess, P., Ito, A., Kawa, S. R., Law, R. M., Loh, Z., Maksyutov, S., Meng, L., Palmer, P. I., Prinn, R. G., Rigby, M., Saito, R., and Wilson, C.: TransCom model simulations of CH<sub>4</sub> and related species: linking transport, surface flux and chemical loss with CH<sub>4</sub> variability in the troposphere and lower stratosphere, *Atmos. Chem. Phys.*, 11, 12813–12837, doi:10.5194/acp-11-12813-2011, 2011.
- Pison, I., Bousquet, P., Chevallier, F., Szopa, S., and Hauglustaine, D.: Multi-species inversion of CH<sub>4</sub>, CO and H<sub>2</sub> emissions from surface measurements, *Atmos. Chem. Phys.*, 9, 5281–5297, doi:10.5194/acp-9-5281-2009, 2009.
- Pison, I., Ringeval, B., Bousquet, P., Prigent, C., and Papa, F.: Stable atmospheric methane in the 2000s: key-role of emissions from natural wetlands, *Atmos. Chem. Phys.*, 13, 11609–11623, doi:10.5194/acp-13-11609-2013, 2013.
- Prinn, R. G., Huang, J., Weiss, R. F., Cunnold, D. M., Fraser, P. J., Simmonds, P. G., McCulloch, A., Harth, C., Reimann, S., Salameh, P., and O'Doherty, S.: Evidence for variability of atmospheric hydroxyl radicals over the past quarter century, *Geophys. Res. Lett.*, 32, L07809, doi:10.1029/2004gl022228, 2005.
- Prinn, R. G., Weiss, R., Fraser, P., Simmonds, P., Cunnold, D., Alyea, F., O'Doherty, S., Salameh, P., Miller, B., and Huang, J.: A history of chemically and radiatively important gases in air deduced from ALE/GAGE/AGAGE, *J. Geophys. Res.*, 105, 17751–17792, 2000.
- Prinn, R. G., Weiss, R. F., Fraser, P. J., Simmonds, P. G., O'Doherty, S., Salameh, P., Porter, L., Krummel, P., Wang, R. H. J., Miller, B., Harth, C., Grealley, B., Van Woy, F. A., Steele, L. P., Mühle, J., Sturrock, G., Alyea, F. N., Huang, J., and Hartley, D. E.: The ALE / GAGE AGAGE Network (DB1001), Carbon Dioxide Information Analysis Center (CDIAC), U.S. Department of Energy (DOE), available at: <http://cdiac.esd.ornl.gov/ndps/alegage.html> (last access: 6 July 2014), 2015.

- Rigby, M., Prinn, R. G., Fraser, P. J., Simmonds, P. G., Langenfelds, R., Huang, J., Cunnold, D. M., Steele, L. P., Krummel, P. B., and Weiss, R. F.: Renewed growth of atmospheric methane, *Geophys. Res. Lett.*, 35, L22805, doi:10.1029/2008GL036037, 2008.
- Rigby, M., Prinn, R. G., O'Doherty, S., Montzka, S. A., McCulloch, A., Harth, C. M., Mühle, J., Salameh, P. K., Weiss, R. F., Young, D., Simmonds, P. G., Hall, B. D., Dutton, G. S., Nance, D., Mondeel, D. J., Elkins, J. W., Krummel, P. B., Steele, L. P., and Fraser, P. J.: Re-evaluation of the lifetimes of the major CFCs and CH<sub>3</sub>CCl<sub>3</sub> using atmospheric trends, *Atmos. Chem. Phys.*, 13, 2691–2702, doi:10.5194/acp-13-2691-2013, 2013.
- Spahni, R., Wania, R., Neef, L., van Weele, M., Pison, I., Bousquet, P., Frankenberg, C., Foster, P. N., Joos, F., Prentice, I. C., and van Velthoven, P.: Constraining global methane emissions and uptake by ecosystems, *Biogeosciences*, 8, 1643–1665, doi:10.5194/bg-8-1643-2011, 2011.
- Spivakovsky, C., Logan, J., Montzka, S., Balkanski, Y., Foreman-Fowler, M., Jones, D., Horowitz, L., Fusco, A., Brenninkmeijer, C., and Prather, M.: Three-dimensional climatological distribution of tropospheric OH: Update and evaluation, *J. Geophys. Res.*, 105, 8931–8980, 2000.
- UNEP: The UNEP Environmental Data Explorer, as compiled from United Nations Environment Programme, United Nations Environment Programme, available at: <http://ede.grid.unep.ch> (last access: 6 July 2014), 2015.
- van der Werf, G. R., Randerson, J. T., Giglio, L., Collatz, G. J., Mu, M., Kasibhatla, P. S., Morton, D. C., DeFries, R. S., Jin, Y., and van Leeuwen, T. T.: Global fire emissions and the contribution of deforestation, savanna, forest, agricultural, and peat fires (1997–2009), *Atmos. Chem. Phys.*, 10, 11707–11735, doi:10.5194/acp-10-11707-2010, 2010.
- Velders, G. J. M.: Description of the RIVM 2-dimensional stratosphere model, RIVM Rapport 722201002, 1995.
- Voulgarakis, A., Naik, V., Lamarque, J.-F., Shindell, D. T., Young, P. J., Prather, M. J., Wild, O., Field, R. D., Bergmann, D., Cameron-Smith, P., Cionni, I., Collins, W. J., Dalsøren, S. B., Doherty, R. M., Eyring, V., Faluvegi, G., Folberth, G. A., Horowitz, L. W., Josse, B., MacKenzie, I. A., Nagashima, T., Plummer, D. A., Righi, M., Rumbold, S. T., Stevenson, D. S., Strode, S. A., Sudo, K., Szopa, S., and Zeng, G.: Analysis of present day and future OH and methane lifetime in the ACCMIP simulations, *Atmos. Chem. Phys.*, 13, 2563–2587, doi:10.5194/acp-13-2563-2013, 2013.
- Voulgarakis, A., Marlier, M. E., Faluvegi, G., Shindell, D. T., Tsigaridis, K., and Mangeon, S.: Interannual variability of tropospheric trace gases and aerosols: The role of biomass burning emissions, *J. Geophys. Res.-Atmos.*, 120, 7157–7173, 2015.
- Wang, J. S., Logan, J. A., McElroy, M. B., Duncan, B. N., Megretskaya, I. A., and Yantosca, R. M.: A 3-D model analysis of the slowdown and interannual variability in the methane growth rate from 1988 to 1997, *Global Biogeochem. Cy.*, 18, 3, doi:10.1029/2003GB002180, 2004.
- Warwick, N. J., Bekki, S., Law, K. S., Nisbet, E. G., and Pyle, J. A.: The impact of meteorology on the interannual growth rate of atmospheric methane, *Geophys. Res. Lett.*, 29, 20, doi:10.1029/2002GL015282, 2002.
- Wennberg, P. O., Peacock, S., Randerson, J. T., and Bleck, R.: Recent changes in the air–sea gas exchange of methyl chloroform, *Geophys. Res. Lett.*, 31, L16112, doi:10.1029/2004GL020476, 2004.
- Yan, X., Akiyama, H., Yagi, K., and Akimoto, H.: Global estimations of the inventory and mitigation potential of methane emissions from rice cultivation conducted using the 2006 Intergovernmental Panel on Climate Change Guidelines, *Global Biogeochem. Cy.*, 23, GB2002, doi:10.1029/2008gb003299, 2009.